Journal of Electrical Engineering, Vol. 74, No. 3, 2023, pp. 210-217

sciendo

PAPER

Sensorless field-oriented control inverter of BLDC motor for copter

Dávid Rau, Tomáš Vršanský

This paper focuses on optimizing the propulsion system, specifically the control aspect. It presents the design of a sensorless inverter with field-oriented control for BLDC motors, primarily intended for copters. The theoretical part covers motor modeling and the design of the control structure, employing field-oriented control and a sensorless approach using back-electromotive force observer to estimate the rotor position. The physical implementation of the control system is based on an electronic inverter with two logical components. The control component utilizes a microprocessor for FOC control and incorporates memory, sensor systems, and peripherals. The power component ensures controlled energy transfer through complementary signals and feedback measurement. Communication between components and with the higher-level system, regarding control and configuration, is also addressed. Finally, the inverter underwent testing on a measurement platform and during copter flights. The measurements focused on motor speed estimation and control performance under load and no-load conditions. The assessment concludes with trust scaling and temperature measurements of the inverter.

Keywords: Drone, copter, BLDC, FOC, vector control, observer, invertor, sensorless

1. Introduction

Drones are currently very popular and find applications in various areas of our lives. Among these drones, copters represent a specific category that offers significant advantages, particularly in inhabited environments. They can maneuver comfortably and do not require large takeoff and landing areas due to their vertical takeoff capabilities. Additionally, copters are known for their modularity and scalability, which allows them to perform various tasks and transport useful payloads.

We are currently participating in a project focused on the transportation of biological material from a medical facility to a laboratory. In this context, the copter appears to be a suitable means of transport. However, the main goal is to ensure the longest possible flight time. The search for alternative energy sources to replace lithium batteries is not feasible due to the required infrastructure. Therefore, we focus on propulsion system optimization, which is a widely used approach for increasing flight time.

The main objective of the optimization is to achieve efficient control of the brushless direct current (BLDC) motor. Currently, the copter uses 6-step commutation for BLDC motor control, which has certain limitations and disadvantages. This method exhibits poor dynamic response and suboptimal energy efficiency, making it less suitable for increasing the flight time of copters. Therefore, our work focuses on the design and implementation of an innovative inverter with sensorless field-oriented control (FOC) for BLDC motors in copters. FOC enables higher energy efficiency, improved dynamic response and overall enhanced motor control characteristics. With this technique, we can optimize the propulsion system and increase the flight time of copters. Compared to the traditional 6-step commutation, FOC offers significant advantages and improves copter performance through superior motor control and more efficient use of energy.

2. Motor model

The development of our inverter design is founded on the mathematical model of the BLDC motor. We acquired the motor model from our prior work in [1]. This model encompasses the entire electrical component of the motor and offers a comprehensive description of its operational characteristics. It is defined by a set of differential equations that accurately capture the behavior of a three-phase motor system during operation. The model's output represents a trapezoidal shape for the back-electromotive force (BEMF) in accordance with the inherent nature of BLDC motors, which is attributed to their salient motor structure. The motor model is derived from [1][2] and is expressed as follows:

$$\frac{d}{dt}i_a = \frac{1}{3L_s}\begin{pmatrix} 2v_{ab} + v_{bc} - 3R_s i_a \\ +\lambda p \omega_m \left(-2\phi'_a + \phi'_b + \phi'_c\right) \end{pmatrix} \quad (1)$$

$$\frac{d}{dt}i_a = \frac{1}{3L_s}\begin{pmatrix} 2v_{ab} + v_{bc} - 3R_s i_a \\ +\lambda p \omega_m \left(-2\phi'_a + \phi'_b + \phi'_c\right) \end{pmatrix} \quad (2)$$

$$\frac{d}{dt}i_c = -\left(\frac{d}{dt}i_a + \frac{d}{dt}i_b\right) \quad (3)$$

$$T_e = p\lambda\left(\phi'_a \cdot i_a + \phi'_b \cdot i_b + \phi'_c \cdot i_c\right) \quad (4)$$

The variables defined in the equations are: phase current (i_x), electromotive force (Φ'_x), phase-to-phase voltage (v_{xy}), stator inductance (L_s), stator resistance (R_s), flux of the permanent magnet (λ), number of pole pairs (p), angular velocity of the rotor (ω_m), and electromagnetic torque (T_e).

For control design, we considered the above-mentioned model in [1] to be nonlinear and complex. Therefore, we proceeded to simplify the model to a linear motor model. The simplification condition assumed of the control point being

Aerobtec, Bratislava, Slovakia
david.rau@aerobtec.com, tomas.vrsansky@aerobtec.com

https://doi.org/10.2478/jee-2023-0027, Print (till 2015) ISSN 1335-3632, On-line ISSN 1339-309X

located at high electrical speeds. This assumption is fulfilled in the case of copters, and the BEMF thus takes on a shape close to a sine wave. As a result, we obtained a simplified model from [1] shown in Fig. 1.

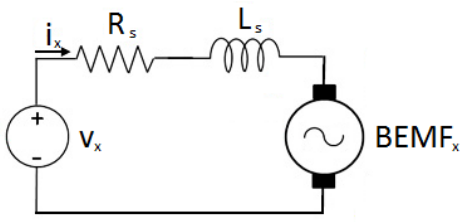

Fig. 1. Simplified model of the motor [1]

The motor model from the source [1] is described by the transfer function $M(s)$ as

$$M(s) = \frac{U(s)}{I(s)} = \frac{\frac{1}{R_S}}{\left(1+\frac{L_S}{R_S}s\right)}. \quad (5)$$

3. Control

We based the control of the entire system on the implementation of FOC for the BLDC motor using the simplified model from the previous chapter. The FOC uses the Clark transformation to convert motor quantities into a two-phase orthogonal system - stator reference frame. It is followed by the Park transformation, which ensured the transfer from the stator reference frame to the rotor reference frame. With these transformations, we have achieved the conversion of alternating motor quantities to direct ones, which represent the basis for the control design. Direct quantities enable the design of control loops without an alternating component. We based the control on the principle of maximizing thrust. Maximization is achieved by maximum torque per ampere strategy (MTPA) that works exclusively with the current control loop. The basic condition of the MTPA strategy is to maintain a 90-degree angle between the vector of the rotor magnetic flux and the stator current [7]. For the expediency of motor control on the copter, cascade control is applied. In our case, the upper loop for the current is the speed control.

A. Current loop

At a lower level of control, there are current controllers that specifically focus on the amplitude and angle of the current vector. The current vector is split into two components: the direct component (i_d) and the quadrature component (i_q). The purpose of controlling the direct component is to maintain it at zero, as it is responsible for generating magnetic flux. Conversely, the objective is to achieve maximum torque, which is associated with the quadrature component, resulting in a desired 90-degree angle between the magnetic flux vectors and the stator current. The control loop comprises PI controllers for each component. The controller parameters, including the proportional gain (K_a) and the integral gain (K_b), are determined based on the transfer function of the closed-loop control system in [3]. By dividing the denominator into two roots and focusing on the linear coefficient, the zero is eliminated from the transfer function, fulfilling the condition that the quadratic coefficient is the product of the roots, and allowing for the determination of one controller parameter [3]. Parameter is in the equation (6).

$$K_b = \frac{R_S}{L_S} \quad (6)$$

We obtain the second controller parameter by substituting it back into the transfer function, resulting in a first-order filter shape dependent on the motor bandwidth [3]. Parameter is in the equation (7).

$$G(s) = \frac{1}{\frac{L_S}{K_a}s+1} \Rightarrow K_a = L_s \cdot Bandwidth(rad/s) \quad (7)$$

The controller parameters we obtained are identical for both the direct and quadrature components of the current, as stated in [1].

B. Speed loop

A higher level of control is achieved with the speed controller, which generates the desired torque as the output and converts it into current for the input of the quadrature current controller. From [1], we obtain the transfer function of the closed-loop control system, where the speed controller takes the form of a PI controller. The parameters of the controller consist of proportional and integral gains, as defined [4][5] in equation (8) and (9).

$$K_c = \frac{1}{\delta K \tau} \quad (8)$$

$$K_d = \frac{1}{\delta^2 \tau} \quad (9)$$

The equation includes the following variables: damping factor (δ), motor constant divided by the moment of inertia (K), and time constant (τ), assuming the presence of a first-order filter as a velocity sensor [1].

C. Sensorless feedback

Feedback is an essential component of the control system. Our system utilizes two types of feedback. The current control loop utilizes a hardware-based current sensor, so we will address the current feedback later. The speed feedback is connected to the Park's transformation, as both depend on the state of the rotor, whether it is the angle or the speed. However, using sensors to measure the rotor position places higher demands on the copter motor, which can be a disadvantage for this type of control. Therefore, we have chosen a sensorless solution based on a software method, where the rotor position is estimated using a state observer.

In the system for estimating quantities, we start with [1], where we have chosen a system consisting of a BEMF observer and a component for calculating the BEMF phase. This entire system operates in the stator reference frame, specifically in a two-phase orthogonal system. The observer is created as a state model of the motor based on the motor model. Based on the

measured input voltage to the motor, the BEMF is estimated as an internal variable, and the output of the model is an estimate of the motor current. This output is compared with the measured current, and the difference is multiplied by the matrix L (P controller) [1]. The component for calculating the phase applies a trigonometric function to the BEMF components from the observer, and the result is the rotor angle. By passing through the derivative term, we can obtain the rotational speed from the rotor angle. The principle of the entire rotor position estimation is shown in Fig. 2.

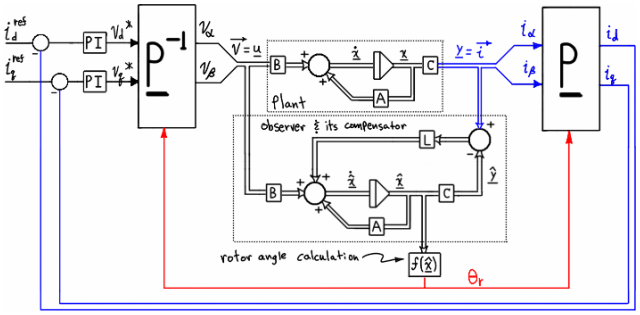

Fig. 2. State-space model of the BEMF observer [6]

Next, we can express the states x, output y, input u, and matrices A, B, C in accordance with [6] using the following equations.

$$x = \begin{bmatrix} i_\alpha \\ i_\beta \\ e_\alpha \\ e_\beta \end{bmatrix} \quad y = \begin{bmatrix} i_\alpha \\ i_\beta \end{bmatrix} \quad u = \begin{bmatrix} v_\alpha \\ v_\beta \end{bmatrix} \tag{10}$$

$$A = \begin{bmatrix} -\frac{R_S}{L_S} & 0 & -\frac{1}{L_S} & 0 \\ 0 & -\frac{R_S}{L_S} & 0 & -\frac{1}{L_S} \\ 0 & 0 & 0 & -\omega \\ 0 & 0 & \omega & 0 \end{bmatrix} \tag{11}$$

$$B = \begin{bmatrix} \frac{1}{L_S} & 0 \\ 0 & \frac{1}{L_S} \\ 0 & 0 \\ 0 & 0 \end{bmatrix} \tag{12}$$

$$C = \begin{bmatrix} 1 & 0 & 0 & 0 \\ 0 & 1 & 0 & 0 \end{bmatrix} \tag{13}$$

The equations involve the following variables: phase currents (i_x), phase voltages relative to neutral (v_x), and BEMF (e_x). By using equations (10), (11), (12), and (13), we applied the state model described in equation (14) according to [1].

$$\frac{\dot{d}}{dt}x = Ax + Bu \qquad y = Cx \tag{14}$$

4. Design of inverter

The physical implementation of the entire control system is based on a real device. This is an electronic inverter that we have developed in full in terms of software and hardware. The inverter is implemented as a two-element system, which consists of a control and a power component. The system of two separate logic units provides a significantly higher degree of variability. Our goal is to make it possible to respond primarily to possible changes in requirements in the power component. The requirements can take the form of changing the power source or the load capacity of the system, while they are primarily focused on the power component. The design is created so that these changes in the power component cause only minimal changes in the software of the control component. The description of the basic functions of the components is in Fig. 3.

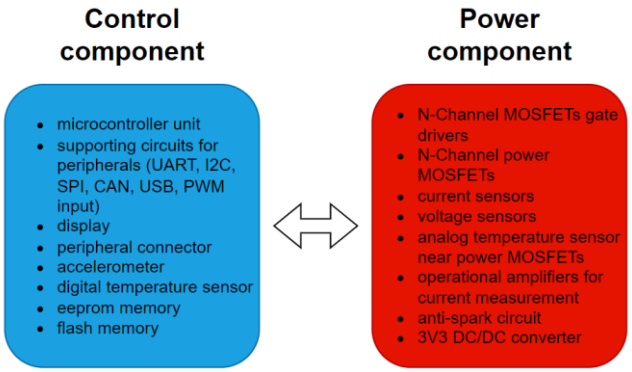

Fig. 3. Block diagram of the inverter

A. Control component

The control component is designed with the basic element, which is a microprocessor from Texas Instruments. The primary task of the microprocessor is the implementation of the FOC control algorithm for the BLDC motor in cooperation with the power component. Another task is the handling of memories, communication, sensor systems and peripherals.

Two types of separate memories are placed on the board. The first memory is 2 kbit in size. It is an EEPROM type memory that can work on the register [8]. This memory is used exclusively for storing a small amount of data. In our case, these are specific parameters of the inverter and the motor. These data are important for the initialization of the entire inverter and equally essential for the creation of a functional model of the motor. The second memory has a large storage space with a size of 64 Mbit, but it can only work on sectors. It is a type of Flash and is used for recording telemetry data or sampling transient effects [9].

The sensor part on the board consists of an accelerometer and a thermometer. The accelerometer is in a 3-axis version [10]. The purpose of its placement on the board is to record vibrations on the copter's arm. Recorded data can be used to analyze unwanted vibrations generated by a mechanically damaged motor. It is also possible to detect a free fall and send this

information to a superior system. The second sensor system is a digital temperature sensor based on a semiconductor thermistor [11]. The sensor provides temperature measurement on the control component. The measured temperature values are used to operate the inverter before it overheats. Likewise, knowledge of these values significantly helps when setting the thermal comfort of the inverter, i.e., design of a suitable cooler.

We designed the control board in such a way that it is possible to install peripherals for informing the user. It is a preparation for fitting an OLED display and an output for connecting localization RGB LEDs.

B. Communication

The functionality of the inverter necessarily needs to communicate with the environment and internally. Therefore, we divided the communication buses used on the inverter into internal and external according to the purpose of communication.

Internal buses are allocated exclusively for communication within the component or mutual communication between the control and power components. We use I2C and SPI synchronous digital buses. The I2C bus serves sensors and peripherals on the control part. The SPI bus is used for configuration and diagnostics of the gate controller on the power component.

External buses perform communication with the superior system, where they ensure the exchange of control signals, configuration signals and telemetry data. Communication is ensured by several channels on the inverter. The simplest communication channel has the form of a PWM (pulse-width modulation) signal fed to the input pin. The mentioned communication is analog and only one-way intended for transmission of the control signal to the inverter. The received signal uses a standard carrier frequency of 50Hz with a filling of 800-2200 us. Another type is the serial line on the USB interface, which offers two-way and digital communication. The line uses a proprietary protocol that enables software configuration of the inverter in addition to control. The transmission speed of the line is set to 921000 baud/s. The maximum permissible frequency of control signals according to the protocol is 400 Hz. The last bus is the CAN bus with the DroneCAN protocol, which has built-in message support for motor inverters [12]. The bus has a transmission speed set to 1Mb/s. As with the serial line, the maximum frequency of the control signal is equal to 400 Hz. Since all external buses are connected to other systems, dangerous current can be carried from that source. The lines are therefore galvanically separated by optocouplers.

C. Control algorithm

We had to correct the conversion of the FOC control algorithm from a mathematical interpretation on a theoretical level for realistically executable software. We conceived the entire system as continuous, but during implementation we converted it into a discrete form. For the system, it was necessary to realize and set the frequencies of control, feedback, and estimation. These frequencies had to be chosen considering the capabilities of the microprocessor and the ability to perform all service processes in Table 1.

TABLE 1 PROCESS FREQUENCIES

Process	Frequency
System clock	60 MHz
PWM output	45 kHz
Feedback measure	15 kHz
Observer estimate	15 kHz
Current control loop	15 kHz
Speed control loop	1 kHz

The frequencies in Table 1 influence the control of the inverter. In addition to measuring the currents, the control performs the reconstruction of their shape. The reconstruction makes it possible to implement corrections between the individual phase currents. Successful reconstruction can only be achieved if aliasing is avoided. We can ensure this state with a lower limit on the electric speed. We set limit to the number of 7 samples limit for the used harmonic waveform. The real device thus receives the first limitation in the form of a maximum electrical speed of ~128000 revolutions per minute.

D. Power component

One of the main activities of the power component is to ensure the controlled transfer of electrical energy from the source to the motor. The control signals come from the control algorithm in the control component. The signals take the form of complementary PWM outputs for the upper and lower transistors. The carrier frequency of the signal is designed regarding its efficiency because the switching of power elements creates losses in the form of waste heat. On the other hand, it is necessary to keep the value large enough so that the signal is sufficiently filtered by the motor and does not cause the motor to jerk. The gate driver of N-channel MOSFET transistors converts these signals to the voltage levels necessary for the correct opening of the transistors. The limit of the current flowing into the gates of the transistors is software configurable. Therefore, it is possible to set the ideal value through the measuring device, preventing unwanted oscillations on the gates of the transistors and ultimately contribute to the efficiency of the control. The gate controller also has a dead time control function. The dead time is the period between switching the external MOSFETs high and low. We set the dead time to the smallest possible value, which still ensured that they do not cross conduct and cause shoot-through. The dead time value on our inverter is 200 ns.

Another content of the power component is the feedback service. Feedback consists of currents and voltages on the individual motor phases. The voltages are measured via an ADC (analog-digital converter) on the microprocessor through a

simple voltage divider with a filter circuit. The currents flowing through the individual phases are measured by the voltage drop on the current shunt resistor. This voltage is amplified by an operational amplifier with a gain of 40VpV, which, in combination with a current shunt resistor with a value of 0.5 mΩ and a 12bit ADC on the microprocessor, represents a current range in the range of +/-82.5A. Phase voltages are measured in the same way as a 12-bit ADC on a microprocessor, and the voltage scale is in the range of 0 - 36.3 V [13]. Voltage measurements include a low-pass filter, which is necessary for the observer to accurately detect the voltage coupling. The filter should be low enough to filter out PWM signals while still allowing high speed voltage the feedback signal pass through the filter. The filter is hardware-tuned to a value of 355.7 Hz. However, the filter also results in a limitation for speed estimation. Therefore, another limitation for the maximum electrical speed has a value of 4 times the filter, i.e., ~85000 revolutions per minute.

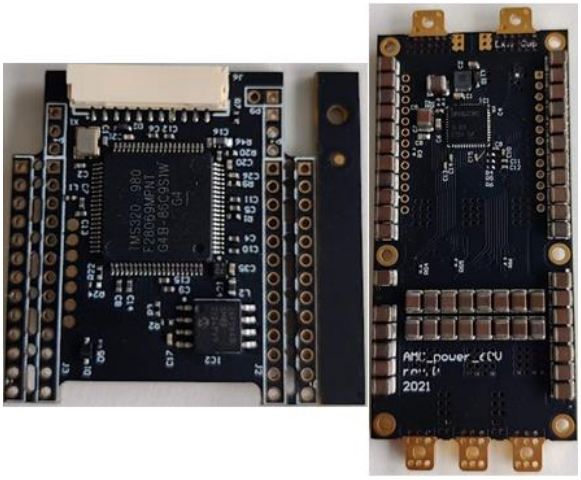

Fig. 4. Real device – control and power component

5. Measurement

The inverter designed by us has been tested. The primary goal of the testing was to verify the full functionality of the inverter from the point of view of use for a copter. Testing was done with the T-Motor AIR2216II, whose parameters are listed in Table 2 [14].

TABLE 2 T-MOTOR AIR2216II PARAMETERS

Quantity	Value
Kv – Coefficient revolutions per volt	920 rpm/V
Maximum current	17 A
Pole pairs	7
Stator resistance	0.061 Ω
Stator inductance	1.173×10^{-5} H
Flux of the permanent magnet	0.00594 Wb

The motor was fitted with a 10-inch T-Motor T1045II propeller designed for this motor [14]. The inverter is powered by a 6-cell LiHV (Lithium Polymer High Voltage) battery with a maximum cell voltage of 4.4V. Parameterization of the motor relates to the setting of the control loops, which are listed in the Table 3.

TABLE 3 CONTROL PARAMETERS

Loop	Controller parameters	
	Proportional Gain	***Integral Gain***
Current	Ka = 0.075	Kb = 0.344
Speed	Kc = 1.0	Kd = 0.078

We performed the tests in a single configuration on a calibrated measuring stand - Tyto Robotics Series 1585 Thrust Stand Bundle. The second way we performed test flights on a copter with our four inverters, where the maximum take-off mass was 2.4 kg.

A. Test without load

We focused the initial tests of the inverter on verifying the functionality of the inverter. The subject of the tests was the verification of the system for unit steps of different sizes, as well as the verification of the quality of the estimation of the motor speed using the observer. We performed the tests on the measuring stand. The measured data comes from the measuring stand and directly from the telemetry of the inverter.

Fig. 5 shows a comparison of the accuracy of the motor speed estimate by the inverter against the speed measured by the stand's optical sensor. The result shows sufficient accuracy, as the difference is in the range of 20-40 rpm, which is negligible compared to the current value in thousands of rpm. The difference is obvious in the form of overshooting the estimate. This difference arises due to the influence of a worse estimate from the measured values, which is significantly more affected by noise and high motor dynamics without load. Another difference is when it drops to zero, when the motor is not actively braked and thus estimation is not possible.

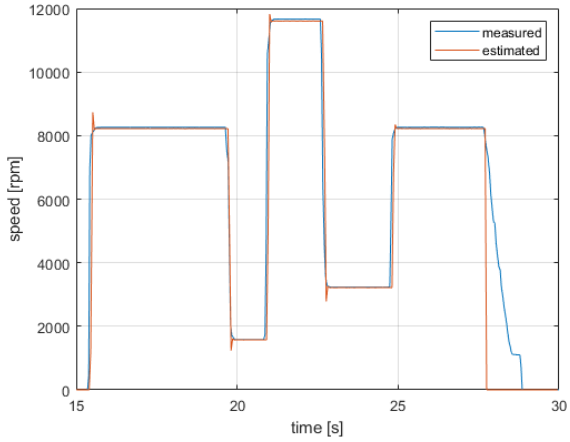

Fig. 5. Comparison of estimated and measured motor speed

Fig. 6represents the control quality without using dynamic limitation. In this case, the motor without load follows the desired value without hesitation. The minimal differences between the steady state values are because we are not directly recording the required speed. This is obtained by calculation from the norm control signal.

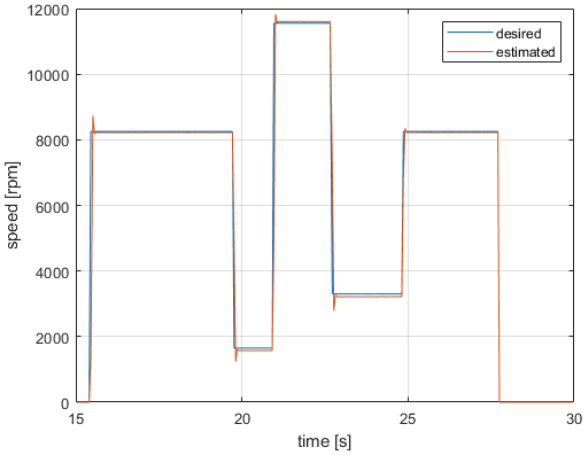

Fig. 6. Comparison of desired and estimated motor speed

B. *Test with load*

We continued testing with a load in the form of a propeller on a measuring stand. Fig. 7 shows speed control, where the applied load already affects the dynamics of the system. In this case, the control is set correctly because there is no overshot, which is unacceptable for the copter motor inverter.

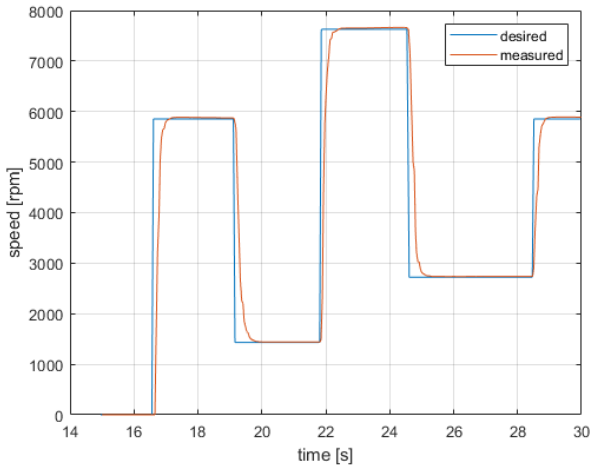

Fig. 7. Comparison of desired and measured motor speed with load

The next chart shows the operating ranges of the test motor with our test copter inverter. The testing was performed in successive jumps of 5% of the control input. As a result, the inverter is adjusted in such a range that one inverter with a motor has a thrust equal to twice the required take-off weight per motor. In this way, we get an overview of the thrust of the propeller, speed, power and current of the motor in Fig. 8.

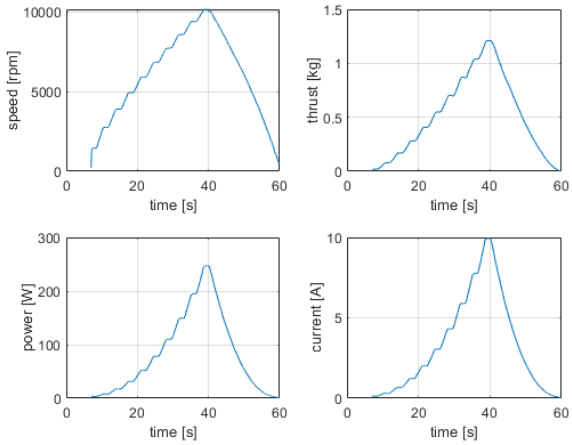

Fig. 8. Overview of speed, thrust, power and current in operating range

C. *Thrust scaling*

Measurements with a load provided insight into the motor's overall working range. However, the output of the inverter with the motor brings non-linearity in the dependence of the thrust on the revolutions. This non-linearity presents a problem for the control of the copter. Therefore, it is necessary to describe this nonlinearity analytically, where approximation by a quadratic function is used. Subsequently, we can provide a coefficient to the control of the copter, which ensures the generation of the inverse characteristic for thrust linearization.

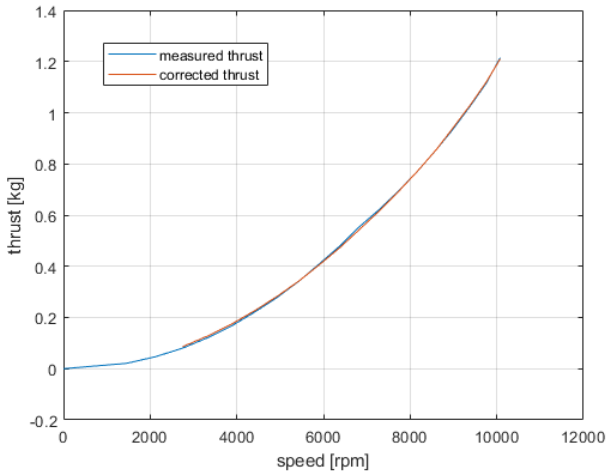

Fig. 9. Measured thrust and corrected thrust as an approximation

The approximation function uses norm values of quantities. The calculation of the coefficient for controlling the copter in Fig. 9 is c = 0.5 defined by (15).

$$thr(spd) = (1 - c) * spd + c * spd^2 \qquad (15)$$

D. Thermal comfort

The last test represents thermal comfort, which records the balance of the inverter with the waste heat. The first was a recording from thermal imaging, where the

Fig. 10shows a view of the control part after 10 minutes with 50% power of the inverter on the measuring stand.

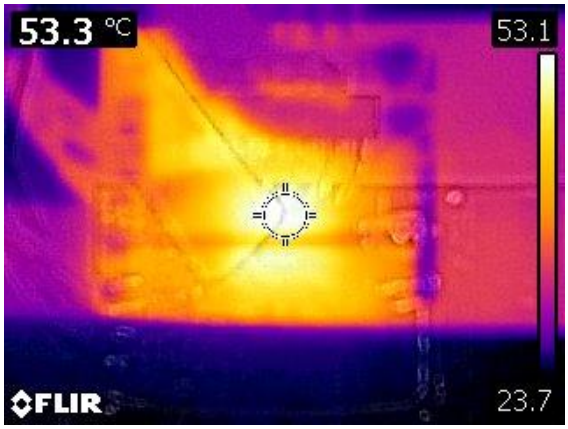

Fig. 10. Measuring the temperature of the inverter by thermal imaging

The second measurement was based on the temperature record during the 6-minute flight of the copter, which consisted of a zig-zag movement in the vertical axis and a gradual horizontal shift. Even with such a dynamic flight, the temperature gradually stabilized in Fig. 11.

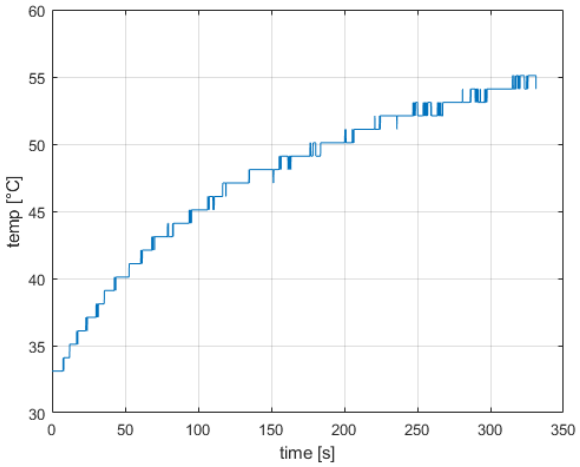

Fig. 11. Temperature behavior during flight

We have managed to maintain a stable thermal comfort of the inverter, which can maintain stable maximum temperatures and thus control within the limits.

6. Conclusion

In the article, we described the design of an inverter for a BLDC motor based on field-oriented control. The theoretical control design is based on a simplified motor model, where we created control loops for speed and current with the MTPA control strategy. We also derived an observer from the motor model to estimate the rotor state, which is crucial for transformation and feedback. Subsequently, we designed a physical inverter consisting of control and power components. During the hardware design, we had to define certain limitations of the theoretical design. Finally, we installed a motor with propeller on the device and adjusted the corresponding parameters for the specific system. With this setup, we performed a series of measurements on a test stand and a copter, focusing on control quality and rotor state estimation. The results of these tests confirmed the designed inverter parameters, although some aspects needed adjustments for copter use, including thrust profile and thermal comfort verification.

Acknowledgement

This article was written thanks to the generous support under the Operational Program Integrated Infrastructure for the project: "Research and development of the applicability of autonomous flying vehicles in the fight against the pandemic caused by COVID-19 ", Project no. 313011ATR9, co-financed by the European Regional Development Fund.

References

[1] D. Rau, J. Rodina, L. Palkovic and P. Hubinsky, "Sensorless Field Oriented Control of BLDC Motors for MAVs," Transactions on Electrical Engineering, vol.4, pp. 91-96, 2015.

[2] MathWorks (1.4.2023). Permanent Magnet Synchronous Machine [online]. Available: https://www.mathworks.com/help/sps/powersys/ref/permanentmagnetsynchronousmachine.html

[3] Dave Wilson (1.4.2023). Teaching Your PI Controller to Behave (Part II) [online]. Available: https://e2e.ti.com/blogs_/b/industrial_strength/posts/teaching-your-pi-controller-to-behave-part-ii

[4] Dave Wilson (1.4.2023). Teaching Your PI Controller to Behave (Part III) [online]. Available: https://e2e.ti.com/blogs_/b/industrial_strength/posts/teaching-you-pi-controller-to-behave-part-iii

[5] Dave Wilson (1.4.2023). Teaching Your PI Controller to Behave (Part IV) [online]. Available: https://e2e.ti.com/blogs_/b/industrial_strength/posts/teaching-your-pi-controller-to-behave-part-iv

[6] James Robert Mevey, Sensorless field oriented control of brushless permanent magnet synchronous motors. Kansas State University, Kansas. 2009.

[7] H. R. Mosaddegh, H. A. Zarchi, Maximum Torque per Ampere Control of Brushless Doubly Fed Induction Machine using Variable Structure Approach. Ferdowsi University of Mashhad, Iran, 2014.

[8] STElectronics. (1.4.2023). Datasheet – I2C bus EEPROM M24C01/02-W M24C01/02-R M24C02-F [online]. Available: https://eu.mouser.com/datasheet/2/389/m24c01_r-1849655.pdf

[9] MicroChip. (1.4.2023). Datasheet – Flash Memorzy SST26WF064C [online]. Available: https://eu.mouser.com/datasheet/2/268/20005430b-1138417.pdf

[10] STElectronics. (1.4.2023). Datasheet – MEMS digital output motion sensor LIS2DH12 [online]. Available: https://www.mouser.sk/datasheet/2/389/lis2dh12-1849850.pdf

[11] NXP. (1.4.2023). Datasheet – Digital temperature sensor and thermal watchdog LM75B [online]. Available: https://www.mouser.sk/datasheet/2/302/LM75B-3138681.pdf

[12] DroneCAN. (1.4.2023). DroneCAN Specification [online]. Available: https://dronecan.github.io

[13] Texas Instruments. (1.4.2023). Datasheet - TMS320F2802x Microcontrollers [online]. Available: https://www.ti.com/lit/ds/symlink/tms320f28027.pdf

[14] T-Motor. (1.4.2023) Specification – AIE GEAR 450II [online]. Available: https://store.tmotor.com/goods.php?id=1220

Received 18 May 2023